22

Synthesis of Novel Nanoparticle - Nanocarbon Conjugates Using Plasma in Ionic Liquid

Toshiro Kaneko and Rikizo Hatakeyama
Tohoku University
Japan

1. Introduction

Since metal and semiconducting nanoparticles have high catalytic activity due to their size effects (Nishikawa et al., 2002), and carbon nanotubes functionalized by foreign atoms and molecules are very fascinating materials in nanoelectronics applications, the various kinds of nanoparticles conjugated with the carbon nanotubes (Georgakilas et al., 2007; Han et al., 2004) could constitute promising nanoelectronics devices such as gas sensors (Kong et al., 2000), field-effect transistors (Kim et al., 2007), and so on. Up to now, electrochemical decoration (Wildgoose et al., 2005), plasma-ion irradiation (Jeong et al., 2003), and supercritical fluid method (Ye et al., 2004) have been extensively utilized for the synthesis of the nanoparticles conjugated with the carbon nanotubes. However, the nanoparticles usually attach to the outside of the carbon nanotubes, and as a result, they easily agglutinate and change in quality by the heat or chemical reactions. Therefore, it has been claimed that the nanoparticles should be intercalated into the interlayer of the bundled carbon nanotubes. Based on these backgrounds, we attempt to develop a novel nanoparticles synthesis method using gas (plasma) / liquid (ionic liquids) interfacial fields under low gas pressures, where the various kinds of the nanoparticles can be generated and intercalated into the carbon nanotubes.

Recently, many works on the gas-liquid interfacial plasmas have been performed as fundamental and applied researches (Bruggeman & Leys, 2009). Among them, the nanoparticle synthesis using the plasma-liquid interfaces (Meiss et al., 2007; Torimoto et al., 2006; Xie & Liu, 2008; Hieda et al., 2008; Koo et al. 2005) is especially advantageous in that toxic stabilizers and reducing agents are unnecessary and the synthesis is continuous during the plasma irradiation. In these methods, although it has been reported that the metal salt is reduced by an electron or an active hydrogen, the optimal plasma conditions in terms of the synthesis rate, size control, and simplicity remain unclear because the inevitable high voltage discharge in the atmospheric pressure and the consequential dynamic behavior of the gas-liquid interface prevent us from analyzing the precise properties of the plasmas in the interfacial region. In this sense, we have claimed that the generation of the static gas-liquid interface under the low gas pressure condition is necessary to clarify the phenomena at the gas-liquid interface for application to the effective and controllable nanoparticle synthesis.

In this chapter, we present the development of a new plasma system to form the spatially and temporally stable plasma-liquid interfacial surface (Baba et al., 2007; Kaneko et al.,

2009a), i.e., a direct current (DC) discharge plasma is generated just above the liquid by applying the DC power to the electrodes immersed in the liquid and located in the gas phase region, and the precise potential structure between these electrodes through the gas-liquid interfacial region is measured. Furthermore, control of the plasma irradiation flux and energy to the liquid is revealed to be useful for the application such as creation of various kinds of nanoparticles (Baba et al., 2009; Kaneko et al., 2009b), and the nanoparticles conjugated with the carbon nanotubes (Baba et al., 2010).

2. Experimental apparatus

For the purpose of the generation of the static and stable plasma contacting with the liquid, we adopt ionic liquids (Seddon, 2003; Rogers & Seddon, 2003) which have recently gotten much attention in the electrochemistry field. The ionic liquids have the interesting characteristics such as their composition consisting of only positive and negative ions, i.e., no neutral solvent, extremely low vapor pressure, high heat capacity, and nonflammability. These characteristics enable us to introduce the ionic liquids to the vacuum system and the discharge plasma. Therefore, the ionic liquids are the most suitable liquid for the formation of nano-composite materials using the discharge plasmas in contact with the liquids.

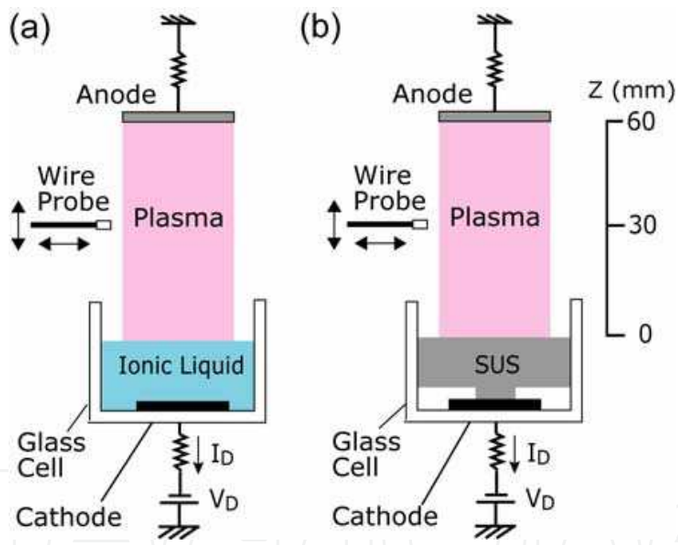

Fig. 1. Schematic diagrams of experimental setup for DC discharge plasmas, where the cathode is set in the glass cell, and is (a) the ionic liquid and (b) the SUS plate. The anode is located at the top of the gas plasma region. These configurations are defined as A-mode.

Figure 1 shows schematic diagrams of experimental setup which has a glass cell of 20 mm in diameter and 10 mm in depth in a cylindrical glass chamber of 15 cm in diameter and 50 cm in length. A cathode electrode which is made of a platinum (Pt) plate with 15 mm diameter is located inside the glass cell and the ionic liquid is introduced on the cathode electrode as shown in Fig. 1(a). Three types of ionic liquids, 1-Ethyl-3-methyl-imidazolium tetrafluoroborate ($[EMI(C_6H_{11}N_2)^+][BF_4^-]$), 1-Butyl-3-methyl-imidazolium tetrafluoroborate ($[BMI(C_8H_{15}N_2)^+][BF_4^-]$), and 1-Hexyl-3-methyl-imidazolium tetrafluoroborate ($[HMI(C_{10}H_{19}N_2)^+][BF_4^-]$), which have different lengths of alkyl chain in the positive ions of them, are introduced into the glass cell, and the amount of the ionic liquid is 1.5 ml.

Removal of the water dissolved in the ionic liquid is performed under the vacuum condition for 2 hours after introducing the ionic liquid into the glass chamber. A DC power is supplied to the cathode electrode in the ionic liquid. On the other hand, a grounded anode electrode which is made of a stainless steel (SUS) plate is set in a gas phase (plasma) region at a distance of 60 mm from the surface of the ionic liquid.

For the purpose of investigating the effects of the ionic liquid on the discharge, the ionic liquid on the Pt plate is replaced by the SUS plate as shown in Fig. 1(b). Here, the surface position of the SUS plate is adjusted to that of the ionic liquid. These discharge configurations, in which the cathode electrode (the Pt plate with the ionic liquid or the SUS plate) is in the glass cell, are defined as "A-mode". Argon gas is adopted as a discharge medium, and the gas pressure P_{gas} is varied from 20 Pa to 80 Pa approximately.

In order to examine the effects of the DC power supplied to the electrode in the ionic liquid on discharge-related phenomena, the cathode electrode is switched to the SUS plate located at the top of the gas plasma region and the Pt plate in the ionic liquid is grounded instead, which is defined as "B-mode" as shown in Fig. 2(a). For the purpose of comparison, the configuration that the SUS plate in the glass cell is grounded, i.e., works as the anode electrode, is also introduced [Fig. 2(b)].

A high voltage probe is directly connected to the cathode electrode to measure the bias voltage of it. A Langmuir probe is inserted at the position of z = 0 - 60 mm to measure parameters of the plasma in contact with the ionic liquid (z = 0: surface of the ionic liquid).

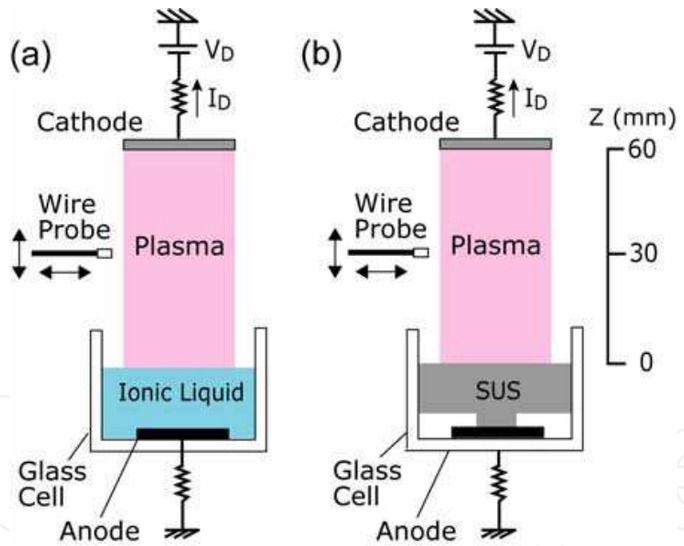

Fig. 2. Schematic diagrams of experimental setup for DC discharge plasmas, where the cathode is located at the top of the gas plasma region. The anode is set in the glass cell, and is (a) the ionic liquid and (b) the SUS plate. These configurations are defined as B-mode.

3. Experimental results and discussion

3.1 Plasma properties

We successfully generate ionic liquid incorporated plasmas at low gas pressures with high stability, similar to normal glow discharge plasmas. Figure 3 shows the photos of the stable DC discharge plasma in A-mode in the regions below the anode electrode and above the

cathode electrodes consisting of the SUS and the ionic liquid (IL) as a function of gas pressure P_{gas}, where the discharge current I_D is fixed to 1 mA. It is found that the cathode glow is clearly observed and its volume becomes small with an increase in the gas pressures, while little emission is observed in the region below the anode electrode. There is little difference in the behavior of the cathode glow between the SUS and IL cathode electrodes.

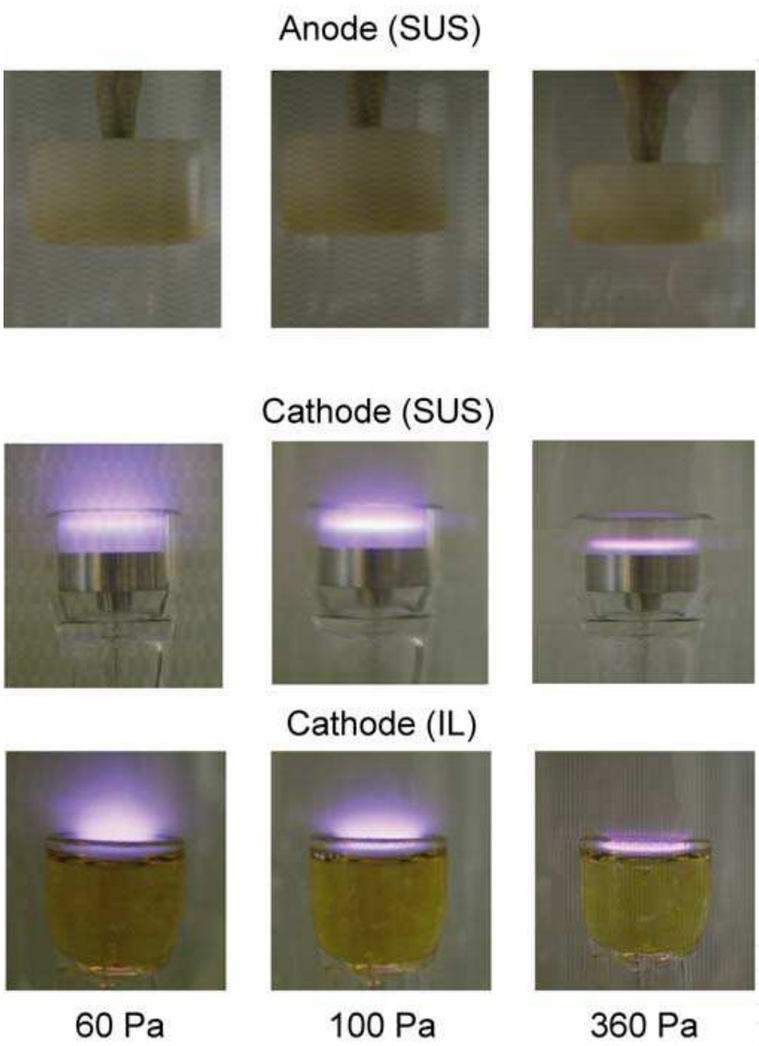

Fig. 3. Photos of the stable DC discharge plasma in A-mode in the regions below the anode electrode and above the cathode electrodes consisting of the SUS and the IL as a function of gas pressure P_{gas}. I_D = 1 mA.

The photos of the discharge plasma in B-mode in the regions below the cathode and above the anodes as a function of gas pressure P_{gas} are given in Fig. 4. The cathode glow is observed below the cathode electrode and its volume becomes small with an increase in the gas pressure in the same way as the case of A-mode. Since the mean free path becomes short with an increase in the gas pressure, the electrons accelerated by the cathode sheath collide with the neutral gas closer to the cathode electrode, and then the glow region is considered to shrink.

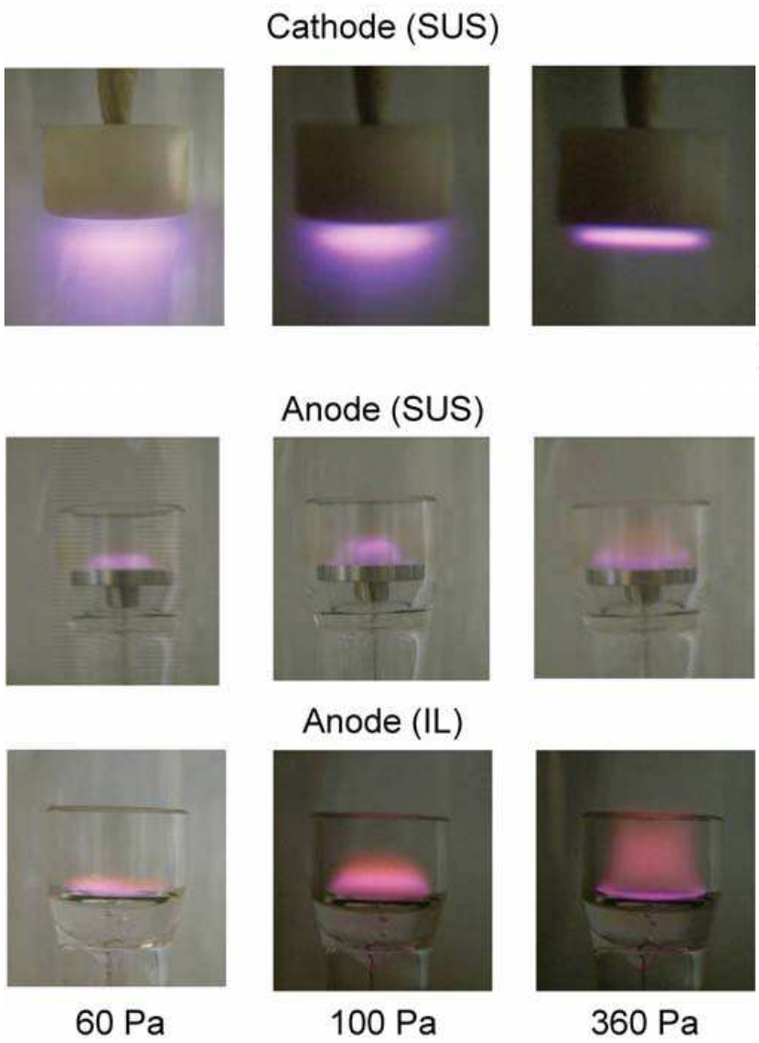

Fig. 4. Photos of the stable DC discharge plasma in B-mode in the regions below the cathode electrode and above the anode electrodes consisting of the SUS and the IL as a function of gas pressure P_{gas}. I_D = 1 mA.

In addition, the anode glow is also observed above both the SUS and IL anode electrodes in the case of B-mode. The volume of the anode glow becomes larger with an increase in the gas pressure, because the recombination occurs more frequently at the high pressures and the anode glow extends to the plasma region. Furthermore, the volume of the anode glow in the IL electrode is larger than that in the SUS electrode. This phenomenon is explainable in terms of the high electron density due to the larger secondary electron emission coefficient of the IL electrode (Kaneko et al., 2009a).

Figure 5 presents axial profiles of the space potential ϕ_s in (a) A-mode and (b) B-mode for P_{gas} = 60 Pa and I_D = 1 mA (discharge current), where the cathode electrodes are the IL (red circles) and the SUS plate (black diamonds). In A-mode, the discharge voltages V_D, i.e., the potentials of the cathode electrode are about –380 V and –540 V when the cathode materials are the IL and SUS, respectively. When the cathode electrode consists of the IL, a large number of secondary electrons are emitted from the IL cathode compared with the SUS

cathode, and therefore, the discharge voltage becomes small for fixed discharge current I_D=1 mA. Furthermore, these many electrons emitted from the IL cathode make the space potential lower than that in the case of the SUS cathode. The space potential in the case of the IL cathode gradually increases around z=40 mm toward the anode electrode. Since the potential difference between the plasma and the IL cathode is about 330 V, the sheath electric field is formed above the IL cathode, giving rise to the electrostatic acceleration of positive ions in the plasma toward the IL, namely ion irradiation on the IL.

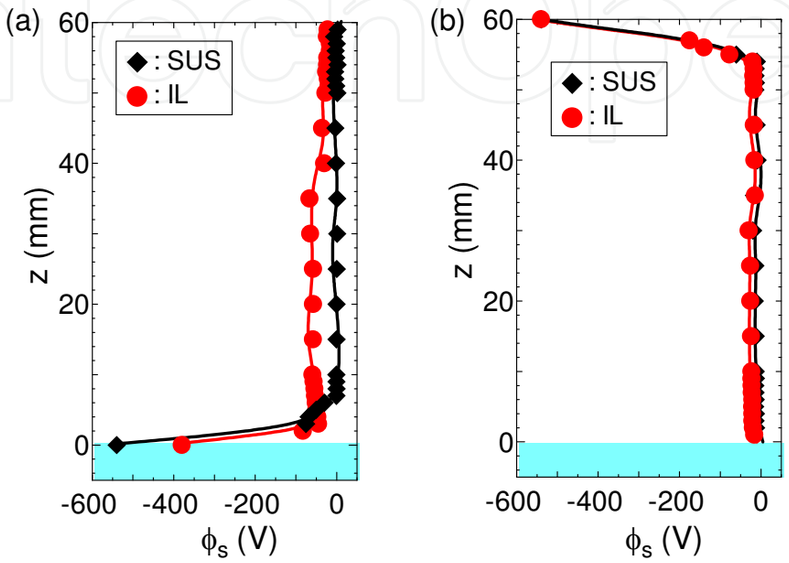

Fig. 5. Axial profiles of the space potential ϕ_s in (a) A-mode and (b) B-mode. P_{Ar} = 40 Pa, I_D=1 mA.

In B-mode, on the other hand, the discharge voltages, i.e., the potentials of the upper SUS cathode electrodes are the same (V_D = –540 V) and the axial profiles of the space potential are almost the same in both the cases with and without the IL. Since the potential in the plasma region is about –20 V, the potential difference between the plasma and the IL anode electrode is relatively small (~ 20 V) and the electric field direction is opposite to that in A-mode. Therefore, the electrons in the plasma are injected into the IL with small energy instead of the positive ion irradiation with high energy. It is also found that the space potential in the case of the IL anode is slightly lower than that of the SUS anode. This result indicates that the secondary electrons are emitted from the IL anode more efficiently than the SUS anode by the injection of the electrons toward the IL, and then, the electron rich condition is realized in the case of the IL anode.

Figure 6 shows axial profiles of the electron density n_e in (a) A-mode and (b) B-mode for P_{gas} = 60 Pa and I_D = 1 mA, where the cathode is the IL (red circles) and the SUS plate (black diamonds). In both A-mode and B-mode, the electron density is large near the cathode electrode and gradually decreases toward the anode electrode. In the case of B-mode, the electron density in the region above the IL anode is much larger than that in the case of the SUS anode, while the electron densities in the region just below the cathode are almost the same independently of the presence of the IL. This increment of the electron density near the IL anode is considered to be attributed to the secondary electron emission from the IL by the collision of the electrons. In the case of A-mode, it is found that the electron density near the

IL cathode is smaller than that in the case of the SUS cathode. Since the discharge voltage in the case of the IL cathode is smaller than that in the SUS cathode case, the energy of electrons accelerated by the potential difference between the plasma and the cathode is small and the ionization rate also becomes low, resulting in the low density near the cathode region. On the other hand, the electron density near the anode electrode has opposite tendency, i.e., the density in the presence of the IL is larger than that in the absence of the IL. Judging from the result of the axial profiles of the space potential [Fig. 5(a)], the potential gradient is generated around z>40 mm in the presence of the IL, and therefore, it is considered that the electrons are accelerated by the electric field and cause the additional ionization near the anode.

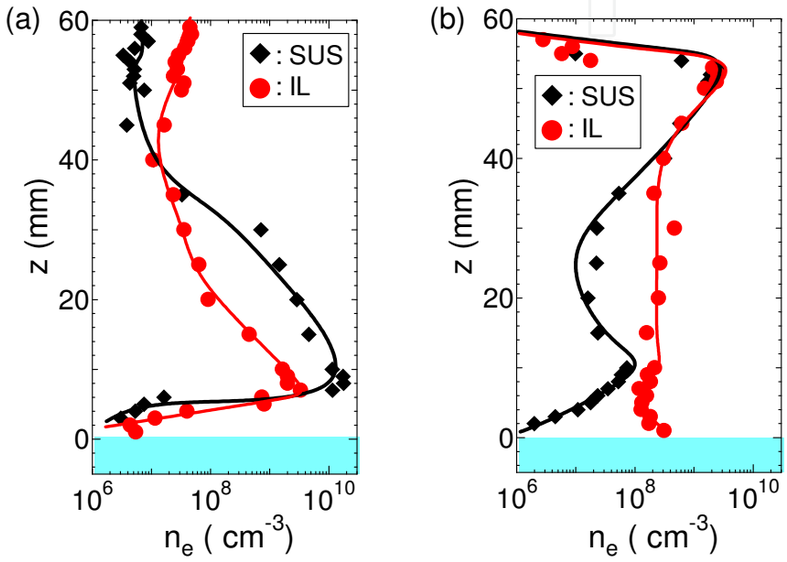

Fig. 6. Axial profiles of the electron density n_e in (a) A-mode and (b) B-mode. P_{Ar} = 40 Pa, I_D=1 mA.

Based on these results, it is found that the secondary electrons are emitted from the IL more efficiently than the SUS electrode by the injection of the electrons to the anode electrode as well as the irradiation of the ions to the cathode electrode. Therefore, the IL electrodes are effective for the synthesis of nanomaterials at the interface between the plasma and the IL.

These ion irradiation and electron injection to the ionic liquid in A- and B-modes, respectively, are expected to affect the discharge in the gas phase region. Therefore, the discharge voltage V_D - current I_D characteristics are measured in both the A- and B-modes, which are presented in Fig. 7, where we change materials of the electrodes in the glass cell, i.e., (a) the cathode electrode in A-mode and (b) the anode electrode in B-mode. When the materials of the cathode electrodes in A-mode are changed between SUS, nickel (Ni), and the ionic liquid ([BMI$^+$][BF_4^-]) [Fig. 7(a)], the discharge current in the case of the ionic liquid is found to be the largest in comparison with those in the cases of Ni and SUS. On the other hand, the change in materials of the anode electrodes in B-mode has no effect on the discharge characteristics as shown in Fig. 7(b). These results suggest that the ionic liquid works as the effective cathode electrode in A-mode and the secondary electrons are emitted from the ionic liquid more efficiently than the SUS and Ni electrodes, because the discharge voltage depends on the amount of the secondary electrons from the cathode electrode in the

case of the usual DC grow discharge. In B-mode, on the other hand, since the material of the cathode electrode is the same as in all cases of changing the anode materials, the discharge voltage-current characteristics do not change in spite of the various kinds of anode electrodes.

The increase in the discharge current in the case of the ionic liquid cathode in A-mode is considered to be attributed to the concentration of the cathode sheath electric field on the ionic liquid surface which is reported to have a string shaped alkyl chain aligned toward the gas-phase region (Sloutskin et al., 2005). The concentration of the electric field causes the efficient ion irradiation to the ionic liquid, resulting in the emission of a large amount of secondary electrons from the ionic liquid surface more than the conventional metal cathodes such as SUS and Ni.

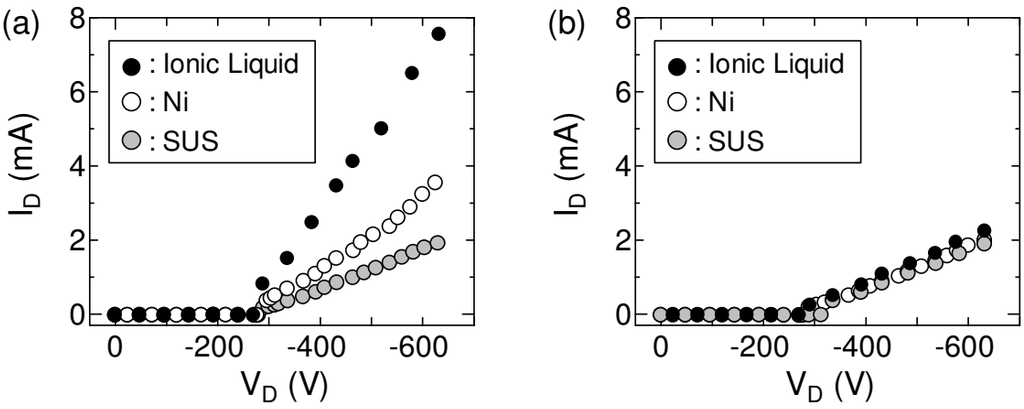

Fig. 7. Dependence of the discharge voltage V_D - current I_D characteristics on the materials of (a) the cathode electrode in A-mode and (b) the anode electrode in B-mode. P_{gas} = 40 Pa. Ionic liquid is [BMI$^+$][BF_4^-].

To confirm the effects of the alkyl chain length of the ionic liquid on the discharge, the discharge voltage V_D – current I_D characteristics are measured with the types of the ionic liquid changed as shown in Fig. 8. In A-mode, the discharge currents in the cases of [HMI$^+$][BF_4^-] and [EMI$^+$][BF_4^-] are the largest and the smallest, respectively. This result shows that the discharge current increases with increasing the length of the alkyl chain in the ionic liquid. These phenomena mean the long alkyl chain contributes to the concentration of the cathode sheath electric field on the ionic liquid surface. The concentration of the electric field causes the efficient ion irradiation to the ionic liquid, resulting in the emission of a larger amount of secondary electrons from the ionic liquid with longer alkyl chain. In B-mode, on the other hand, since the material of the cathode electrode is the same as in all cases of changing the ionic liquids, the discharge voltage- current characteristics do not change in spite of the various kinds of ionic liquids as the anode electrodes.

Figure 9 shows ultraviolet-visible (UV-vis) absorption spectra of the ionic liquid with the ion irradiation energy E_i as a parameter and the spectrum peak intensity at the wavelength of 297 nm as a function of E_i in A-mode, where I_D = 1 mA and the plasma irradiation time t = 2 min. The ion irradiation energy E_i is determined by the potential difference between the plasma and the ionic liquid cathode, which is almost equivalent to the discharge voltage, and control of E_i with the discharge current I_D kept constant is realized by changing the argon gas pressure.

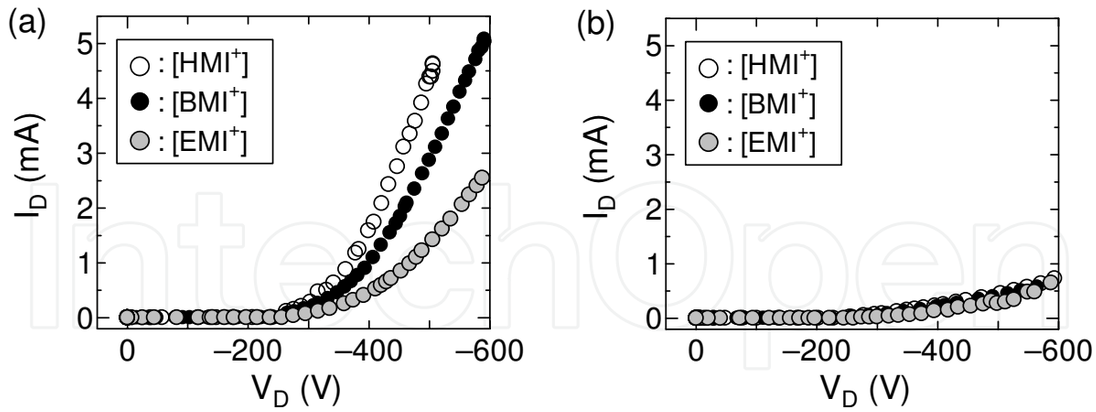

Fig. 8. Dependence of the discharge voltage V_D - current I_D characteristics on the types of the ionic liquids as (a) the cathode electrode in A-mode and (b) the anode electrode in B-mode. P_{gas} = 40 Pa.

The spectrum peak intensity at 297 nm gradually increases with an increase in E_i, which corresponds to the phenomenon that the color of the ionic liquid gradually changes into thick yellow. Since these phenomena are not observed in B-mode, the increase in the absorption peak intensity is caused by the newly-generated bond due to the dissociation of the ionic liquid, which is enhanced by the increase in the ion irradiation energy. Therefore, the molecule structure of the ionic liquid can be varied by the ion irradiation with high energy in A-mode, in which the positive ions in the gas phase plasma are convincingly accelerated by the sheath electric field formed just above the ionic liquid cathode. We emphasize that this ion irradiation to the ionic liquid has the possibility to realize an effective reaction for the material synthesis at the gas-liquid interface.

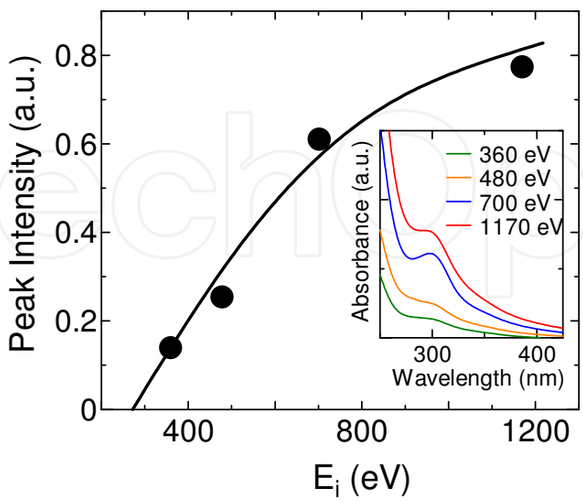

Fig. 9. Peak intensity of UV-Vis absorption spectra of the ionic liquid ([BMI^+][BF_4^-]) at 297 nm as a function of the ion irradiation energy E_i in A-mode. I_D = 1 mA, t = 2 min. Inset is the absorption spectra with E_i as a parameter.

To investigate whether the species in the plasma is changed by the ion irradiation to the IL, optical emission spectra (OES) in the gas plasma region are measured as shown in Fig. 10, where the IL and SUS plate are used as (a) the cathode electrode in A-mode and (b) the anode electrode in B-mode. In A-mode, the spectrum peak at 390 nm, which corresponds to methylidyne radical (CH), is observed only in the presence of the IL [Fig. 10(a)]. In B-mode, on the other hand, the CH peak is not clear both in the presence and absence of the IL.

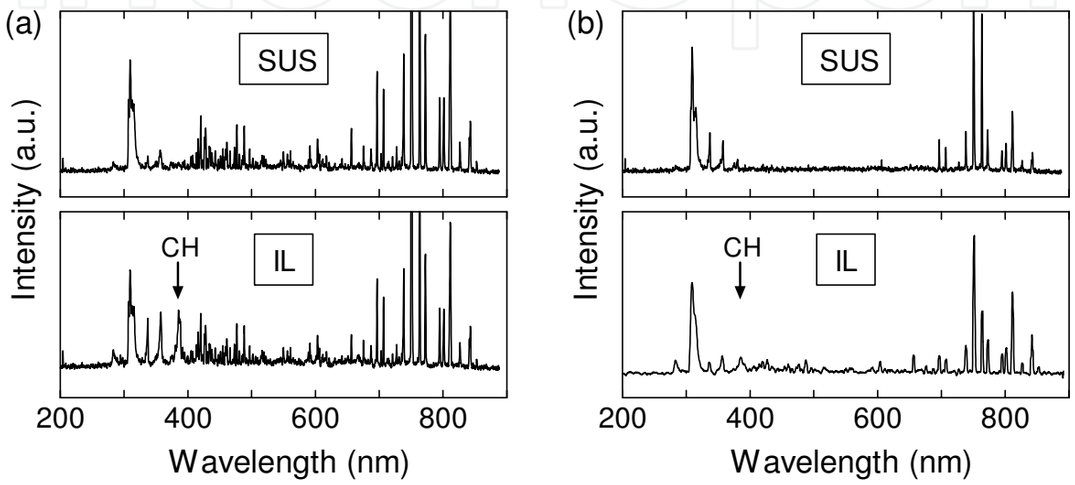

Fig. 10. Optical emission spectra in the gas plasma region in (a) A-mode and (b) B-mode, where the cathode electrode is the IL (bottom figures) and the SUS plate (upper figures). P_{gas} = 60 Pa, I_D = 2 mA.

These phenomena can be explained by a process that the plasma ion irradiation with high energy causes the dissociation of the alkyl-chain of the IL and the dissociated CH is transported to the gas plasma region from the IL region. In these OES spectra, we can find the OH (308 nm) peak in both the cases of A-mode and B-mode. This peak comes from the tiny amount of water included in the IL as an impurity, which is evaporated and dissociated in the gas plasma region not only in A-mode but also in B-mode. This phenomenon is one of the evidence that the CH peak observed only in A-mode is caused by the high-energy ion irradiation to the IL.

3.2 Synthesis of nanoparticles

Using this ion irradiation, gold (Au) nanoparticles are synthesized in the ionic liquid by the reduction of Au chloride such as $HAuCl_4 \cdot 3H_2O$. Figure 11 gives transmission electron microscopy (TEM) images of the Au nanoparticles synthesized in (a) A-mode and (b) B-mode for P_{Ar} = 60 Pa, I_D = 1 mA, and t = 40 min. In both the cases, Au nanoparticles can be formed, however, it is found that, in A-mode, the diameter of the nanoparticle is averagely smaller and the particle number is larger than that in B-mode.

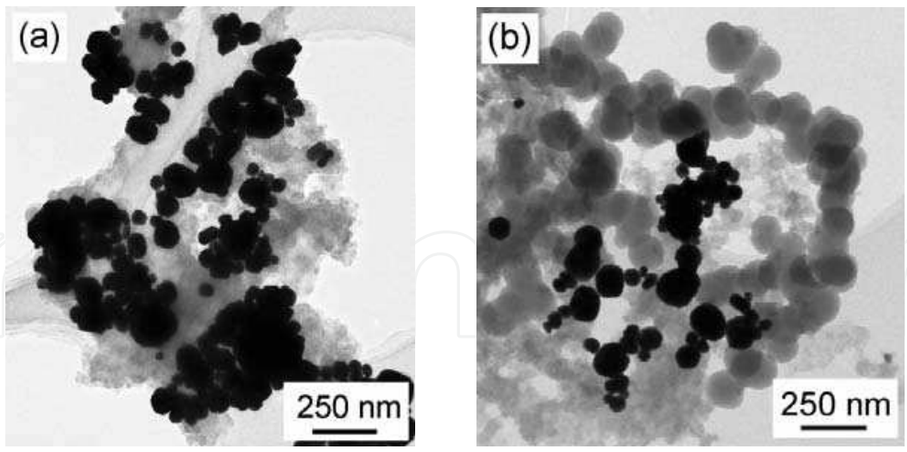

Fig. 11. TEM images of the Au nanoparticles synthesized in (a) A-mode and (b) B-mode. P_{Ar} = 60 Pa, I_D = 1 mA, t = 40 min.

The reduction reaction of the Au ions is caused by the electrons injected from the plasma in B-mode, while the reduction is considered to be caused by hydrogen radical H* in A-mode, which is generated by the dissociation of the ionic liquid. In our system, the Au nanoparticles are synthesized by firstly nucleation of the Au atoms after reduction of the Au chlorides and secondly growth of the nucleus due to attachment of the Au atoms. The density of the nucleus in A-mode is expected to be larger than that in B-mode, because the hydrogen radical effectively reduces the Au chlorides compared with the electron. Therefore, it is considered that the number of Au atoms attached to one nucleus in the growth phase in A-mode is smaller than that in B-mode, resulting in the averagely small diameter and large density of the Au nanoparticles in A-mode.

Since nanoparticles with diameter less than 100 nm are known to cause localized surface plasmon resonance, visible absorption spectra are obtained for a quantitative observation of the Au nanoparticle concentration. Figure 12(a) shows visible absorption spectra of the nanoparticles produced by the Ar plasmas in A-mode with E_i as a parameter. An absorption peak appears around 540 nm, corresponding to Au nanoparticle plasmon resonance and the absorption peak is obviously enhanced with an increase in E_i.

The spatially averaged number density N_p of the synthesized Au nanoparticles, which is counted from the TEM images is presented in Fig. 12(b) as a function of the ion irradiation energy E_i. It is found that N_p monotonically increases with an increase in E_i. The Ar ion can penetrate into the ionic liquid more deeply with an increase in the irradiation energy, resulting in enhancement of the generation of the hydrogen radicals. These increased hydrogen radicals affect the reduction of Au ions. The synthesis efficiency of the Au nanoparticles can be controlled by the irradiation energy of inert gas ions such as Ar.

Finally, we try to control the size of and distance between nanoparticles using the gas-liquid interfacial plasmas. In the beginning, the Au nanoparticles are synthesized using a deferent kind of ionic liquid (1-Butyl-3-methyl-imidazolium chloride, $[BMI(C_8H_{15}N_2)^+][Cl^-]$), which has lager viscosity compared with conventional $[BMI^+][BF_4^-]$. Figure 13(a) shows a TEM image of the synthesized Au nanoparticles, the diameter distribution of which is measured

and plotted in Figs. 13(b) and 13(c). The Au nanoparticles with diameter in the range of 3-7 nm are observed to be formed, which are much smaller than those in the case of conventional ionic liquid [BMI$^+$][BF$_4^-$]. Since the viscosity of [BMI$^+$][Cl$^-$] is larger than that of [BMI$^+$][BF$_4^-$], growth and aggregation of the Au nanoparticles are suppressed by the ionic liquid with high viscosity, resulting in the formation of the small and relatively mono-dispersed nanoparticles.

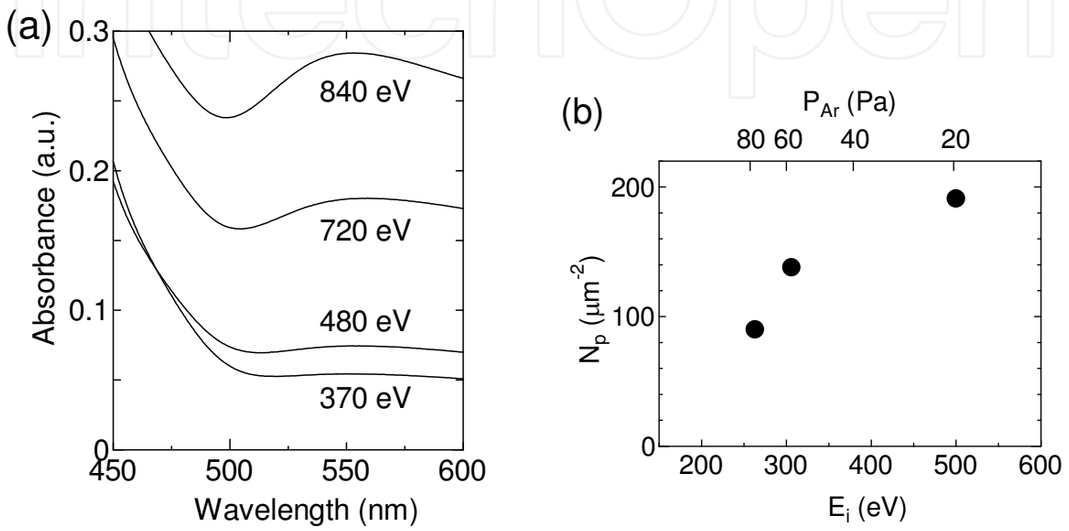

Fig. 12. (a) UV-vis absorption spectra of the Au nanoparticles produced by Ar plasmas as a function of ion irradiation energy E_i in A-mode. I_D = 1 mA, t = 7 min. (b) Spatially averaged number density N_p of the synthesized Au nanoparticles as a function of ion irradiation energy E_i in A-mode. I_D = 1 mA, t = 40 min.

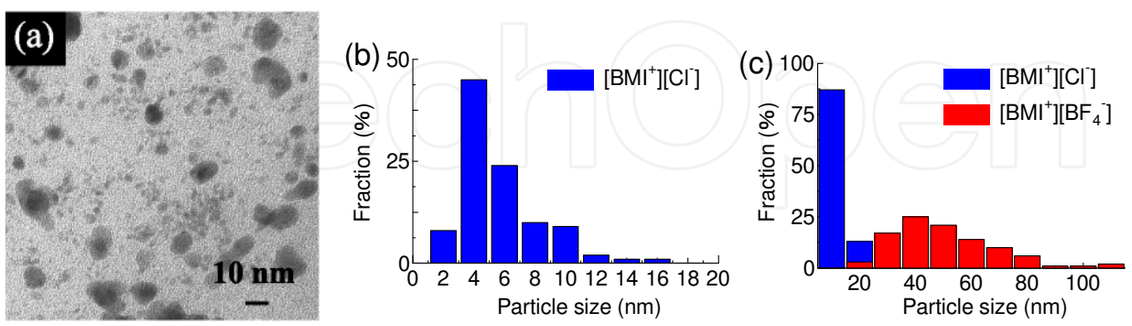

Fig. 13. (a) TEM images of the Au nanoparticles synthesized using the ionic liquid [BMI$^+$][Cl$^-$]. P_{Ar} = 60 Pa, I_D = 1 mA, t = 15 min. (b) Particle size distribution of the Au nanoparticles synthesized in the ionic liquid [BMI$^+$][Cl$^-$] estimated by TEM image in Fig. 13(a). (c) Comparison of the particle size distributions between the cases of [BMI$^+$][Cl$^-$] and [BMI$^+$][BF$_4^-$].

To control the size of nanoparticles, we attempt to make highly-ordered Au and palladium (Pd) nanoparticles using the single-walled carbon nanotubes (SWNTs) as a template. The bundled SWNTs are impregnated with the Au or Pd chloride dissolved in the ionic liquid, and are exposed to the plasma. As a result, the Au or Pd chloride is reduced inside the bundles of the SWNTs by the plasma irradiation and the Au or Pd nanoparticles are synthesized. Since the SWNTs inhibit the agglomeration of the nanoparticles due to their small inside space, the uniform nanoparticles are expected to be synthesized. Figure 14 presents the TEM image of (a) Au and (c) Pd nanoparticles synthesized between the SWNTs in the ionic liquid for P_{Ar} = 60 Pa, I_D = 1 mA, and t = 15 min, and (b) particle size distribution of Au nanoparticles onto the SWNTs estimated by TEM image in Fig. 14(a). It is found that highly-ordered, high-density, mono-dispersed, and small-seized (~ 2 nm) metal nanoparticles are synthesized by controlling the gas-liquid interfacial plasmas.

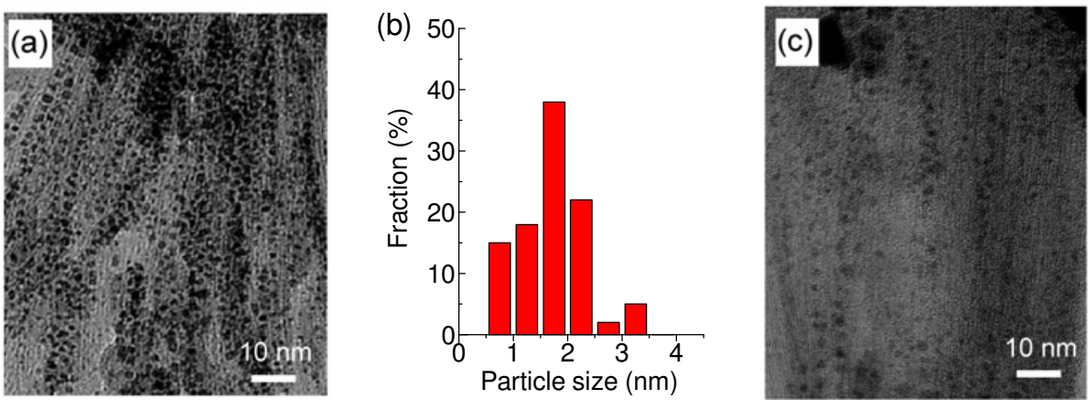

Fig. 14. TEM images of (a) Au and (c) Pd nanoparticles synthesized using the SWNTs as a template. P_{Ar} = 60 Pa, I_D = 1 mA, t = 15 min. (b) Particle size distribution of Au nanoparticles onto the SWNTs estimated by TEM image in Fig. 14(a).

To synthesize distance-controlled nanoparticles, we attempt to make the Au nanoparticles using the functionalized single-walled carbon nanotubes (f-SWNTs) controlled by the irradiation of the gas-liquid interfacial discharge plasma. The SWNTs are dispersed in a new kind of ionic liquid (2-Hydroxyethylammonium formate) which consists of carboxyl groups, and the plasma is irradiated to the IL. The plasma ions or electrons can dissociate the IL and the dissociated carboxyl groups bond to the surface of the SWNTs. This functionalization of the SWNTs using the gas-liquid interfacial plasmas is very easy, fast, and controllable. When chlorauric acid trihydrate ($HAuCl_4 \cdot 3H_2O$) is dissolved in the IL with the functionalized SWNTs, the Au chloride is reduced by the IL and the Au nanoparticles are selectively synthesized on the carboxyl groups bonding to the SWNTs. Since the density of the carboxyl groups on the SWNTs can be controlled by the plasma irradiation parameter, such as irradiation energy, flux, time, and so on, the density of the Au nanoparticles can also be controlled.

Figure 15 presents transmission electron microscope (TEM) images of the Au nanoparticles synthesized on the f-SWNTs, which have been treated in the IL for plasma irradiation time (b) t = 1 min and (c) t = 10 min, P_{Ar} = 60 Pa, and I_D = 1 mA. Here the TEM image of the f-SWNTs which are not previously treated by the plasma irradiation is also present as a reference in Fig. 15(a). It is found that the high density and mono-dispersed Au nanoparticles are synthesized on the f-SWNTs when the SWNTs are previously treated by the plasma irradiation, while only a few Au nanoparticles are observed on the f-SWNTs in the absence of the plasma irradiation. In addition, the distance between the Au nanoparticles becomes small with an increase in the plasma irradiation time. This result means that the distance between the Au nanoparticles can be controlled by functionalization of the SWNTs using the plasma irradiation in the ionic liquid.

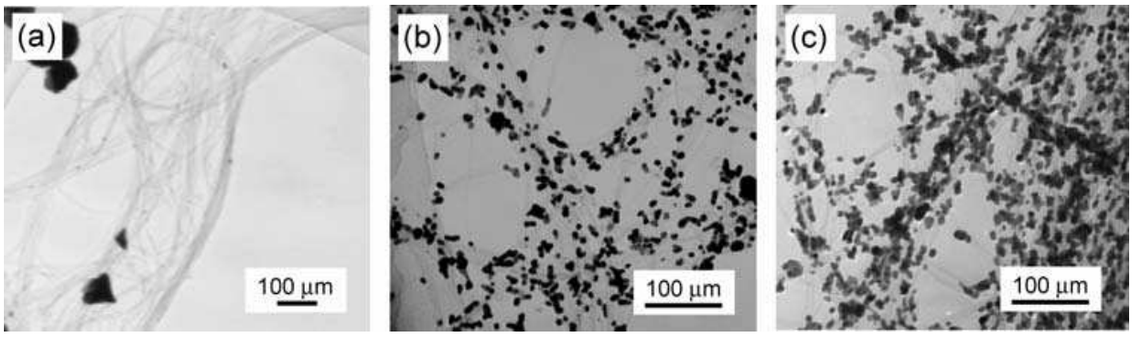

Fig. 15. TEM images of Au nanoparticles synthesized using the functionalized SWNTs, which are treated by the plasma irradiation in the ionic liquid for (a) 0 min, (b) 1 min, and (c) 10 min. P_{Ar} = 60 Pa, I_D = 1 mA.

4. Conclusion

A direct current (DC) discharge plasma has been generated just above the ionic liquid by applying the DC voltage to the ionic liquid as the cathode electrode against a grounded anode electrode set in the gas phase region. On the other hand, the DC discharge plasma between the ionic liquid anode electrode and the negatively biased SUS cathode electrode in the gas phase region is also stably generated.

Using these gas-liquid interfacial plasmas, the precise potential and density structures and the resultant plasma ion and electron irradiations to the ionic liquid are revealed. In addition, it is found that the secondary electrons are efficiently emitted from the ionic liquid electrode by the irradiation of the electrons as well as the high energy ions, and the effects of the secondary electrons on the discharge are clarified. The alkyl chain of the ionic liquid is revealed to play an important role in the secondary electron emission in terms of the concentration of the sheath electric field on the ionic liquid surface.

This ion irradiation is found to be effective for the synthesis of metal nanoparticles in comparison with the conventional electron irradiation system, and has the possibility of application to the synthesis of the various kinds of size- and yield-controlled nanoparticles.

Furthermore, using the plasma irradiation method with single-walled carbon nanotubes as a template, the high density, mono-dispersed, and highly-ordered metal nanoparticles are synthesized by controlling the gas-liquid interfacial plasmas.
The results lead to creating innovative conjugates of carbon nanotubes and nanoparticles, which are expected to be applicable to nanoelectronics and biomedical nanotechnology.
The authors thank Prof. K. Tohji, K. Motomiya, T. Miyazaki, and H. Ishida for their technical assistance. We express our gratitude to Dr. K. Baba, Dr. Q. Chen, and T. Harada, for their collaboration.

5. References

Baba, K.; Kaneko, T. & Hatakeyama, R. (2007). *Appl. Phys. Lett.*, Vol. 90, pp. 201501-1-3, 2007.
Baba, K.; Kaneko, T. & Hatakeyama, R. (2009). *Appl. Phys. Express*, Vol. 2, pp. 035006-1-3, 2009.
Baba K.; Kaneko T.; Hatakeyama R.; Motomiya K. & Tohji K. (2010). *Chem. Commun.* Vol. 46, pp. 255-257, 2010.
Bruggeman P. & Leys, C. (2009). *J. Phys. D: Appl. Phys.*, Vol. 42, pp. 053001-1-28, 2009.
Georgakilas V.; Gournis D.; Tzitzios V.; Pasquato L.; Guldie D. M. & Prato M. (2007). *J. Mater. Chem.* Vol. 17, pp. 2679–2694, 2007.
Han L.; Wu W.; Kirk F. L.; Luo J.; Maye M. M.; Kariuki N. N.; Lin Y.; Wang C. & Zhong C.-J. (2004). *Langmuir* Vol. 20, pp. 6019-6025, 2004.
Hieda, J.; Saito, N. & Takai, O. (2008). *J. Vac. Sci. Technol. A*, Vol. 26, pp. 854-856, 2008.
Jeong, G-H.; Hatakeyama, R.; Hirata, T.; Tohji, K.; Motomiya, K.; Yaguchi, T. & Kawazoe, Y. (2003). *Chem. Commun.*, pp.152-153, 2003.
Kaneko, T.; Baba, K. & Hatakeyama, R. (2009a). *J. Appl. Phys.*, Vol. 105, pp. 103306-1-5, 2009.
Kaneko, T.; Baba, K.; Harada, T. & Hatakeyama, R. (2009b). *Plasma Proc. Polym.*, Vol. 6, pp. 713-718, 2009.
Kim, H.; Kim, B.; Kim, J.; Lee, J. & Park, N. (2005). *Appl. Phys. Lett.*, Vol. 91, pp. 153113-1-3, 2007.
Kong, J.; Franklin, N. R.; Zhou, C.; Chapline, M. G.; Peng, S.; Cho, K. & Dai, H. (2000). *Science*, Vol. 287, pp. 622-625, 2000.
Koo I. G.; Lee M. S.; Shim J. H.; Ahn J. H. & Lee W. M. (2005). *J. Mater. Chem.* Vol. 15, pp. 4125-4128, 2005.
Meiss, S. A.; Rohnke, M.; Kienle, L.; Zein El Abedin, S.; Endres, F. & Janek, J. (2007). *ChemPhysChem*, Vol. 8, pp. 50-53, 2007.
Nishihata, Y.; Mizuki, J.; Akao, T.; Tanaka, H.; Uenishi, M.; Kimura, M.; Okamoto, T. & Hamada, N. (2002). *Nature*, Vol. 418, pp. 164-167, 2002.
Rogers R. D. & Seddon K. R. (2003). *Science* Vol. 302, pp. 792-793, 2003.
Seddon, K. R. (2003). *Nature Mater.*, Vol. 2, pp. 363-365, 2003.
Sloutskin, E.; Ocko, B.M.; Tamam, L.; Kuzmenko, I.; Gog, T. & Deutsch, M. (2005). *J. Am. Chem. Soc.*, Vol. 127, pp. 7796-7804, 2005.
Torimoto T.; Okazaki K.; Kiyama T.; Hirahara K.; Tanaka N. & Kuwabata S. (2006). *Appl. Phys. Lett.* Vol. 89, pp. 243117-1-3, 2006.
Wildgoose, G. G.; Banks, C. E. & Compton, R. G. (2005). *Small*, Vol. 2, pp. 182-193, 2005.
Xie Y. B. & Liu C. J. (2008). *Plasma Process. Polym.* Vol. 5, pp. 239-245, 2008.

Ye, X.; Lin, Y.; Wang, C.; Engelhard, M. H.; Wang, Y. & Wai, C. M. (2004). *J. Mater. Chem.*, Vol. 14, pp. 908-913, 2004.

Ionic Liquids: Theory, Properties, New Approaches
Edited by Prof. Alexander Kokorin

ISBN 978-953-307-349-1
Hard cover, 738 pages
Publisher InTech
Published online 28, February, 2011
Published in print edition February, 2011

Ionic Liquids (ILs) are one of the most interesting and rapidly developing areas of modern physical chemistry, technologies and engineering. This book, consisting of 29 chapters gathered in 4 sections, reviews in detail and compiles information about some important physical-chemical properties of ILs and new practical approaches. This is the first book of a series of forthcoming publications on this field by this publisher. The first volume covers some aspects of synthesis, isolation, production, modification, the analysis methods and modeling to reveal the structures and properties of some room temperature ILs, as well as their new possible applications. The book will be of help to chemists, physicists, biologists, technologists and other experts in a variety of disciplines, both academic and industrial, as well as to students and PhD students. It may help to promote the progress in ILs development also.

InTech Europe
University Campus STeP Ri
Slavka Krautzeka 83/A
51000 Rijeka, Croatia
Phone: +385 (51) 770 447
Fax: +385 (51) 686 166
www.intechopen.com

InTech China
Unit 405, Office Block, Hotel Equatorial Shanghai
No.65, Yan An Road (West), Shanghai, 200040, China
中国上海市延安西路65号上海国际贵都大饭店办公楼405单元
Phone: +86-21-62489820
Fax: +86-21-62489821

IntechOpen